KOSZALIN UNIVERSITY OF TECHNOLOGY
POLITECHNIKA KOSZALIŃSKA

Monograph

RESEARCH AND MODELLING IN CIVIL ENGINEERING 2017

Edited by
Jacek Katzer and Krzysztof Cichocki

KOSZALIN 2017

MONOGRAPH NO 338
FACULTY OF CIVIL ENGINEERING,
ENVIRONMENTAL AND GEODETIC SCIENCES

ISSN 0239-7129
ISBN 978-83-7365-474-7

Chairman of the University Editorial Board
Zbigniew Danielewicz

Editors
Jacek Katzer, Krzysztof Cichocki
Koszalin University of Technology, Poland

Reviewers
Jacek Gołaszewski – Silesian University of Technology, Poland
Izabela Major – Częstochowa University of Technology, Poland

Technical editor
Czesław Suchocki

Website editor
Mariusz Ruchwa

Linguistic consultations
Ewa Sokołowska-Katzer

Typesetting
Czesław Suchocki

Cover design
Tadeusz Walczak
(Photo by *Jacek Katzer*)

KOSZALIN UNIVERSITY OF TECHNOLOGY PUBLISHING HOUSE
75-620 Koszalin, Racławicka 15-17, Poland

Koszalin 2017, 1st edition, publisher's sheet 7,8, circulation 100 copies
Printing: INTRO-DRUK, Koszalin, Poland

Table of contents

7. Impedance spectroscopy, a method to determine physical and chemical properties of construction materials

Miroslav Lunak[1], Ivo Kusak[1]

[1] *Institute of Physics, Faculty of Civil Engineering, Brno University of Technology, Veveri 95, 602 00 Brno, Czech Republic*

7.1. Introduction

Impedance spectroscopy (IS) is a method that employs the impedance frequency dependence to characterize various solids and liquids. To carry out the characterization, IS employs the impedance and phase versus frequency plots, or the so called Nyquist plot, i.e., displaying the impedances in the complex plane throughout the entire frequency range. IS has become a popular method of material research and development, requiring relatively simple electric measurements, which are non-destructive in most cases, and can be automated easily.

To characterize polarization processes, permittivity and impedance are most frequently used in practical applications. As follows from Maxwell's material equations (Szántó 2003), the permittivity is a proportionality constant between the electric field intensity vector and the electric induction vector. An analogous approach can be used to express the impedance and its components.

An ideal dielectric is made up of a substance containing only charges that are bound by electrostatic forces. A real dielectric differs from the ideal one by free electric charges which are causing an undesirable electric conductivity. The physics of dielectric deals with the motion of electric charges. Only electric polarization takes place in ideal dielectrics. Under the influence of an electric field, bound charges shift from their equilibrium positions by a short, limited distance. If the substance contains polar molecules, the electrically bound charges are oriented in the direction of the electric field (Palai-Dany 2009).

Different polarization mechanisms are distinguished with regard to the state and behaviour of the dielectrics in an electric field. Several different polarization types frequently happen to occur simultaneously, stronger mechanisms overlapping the weaker ones (Kocman 1971).

There are a number of the impedance measuring methods. In this paper, we describe a new method, designed by ourselves, to measure and analyse physical and chemical properties of construction materials, indicating the equations and circuit diagrams employed.

The impedance being a complex quantity, at least two related quantities must be measured to determine the impedance. The quantities most frequently used are the electric resistance and the phase change across the unknown impedance. The measuring methods differ from each other in several factors, which are above all the price, frequency and impedance range and automated measurement feasibility.

7.2. Measuring systems and block diagrams

Following devices have been used for the testing of building materials by means of the impedance spectroscopy method: Agilent 33220A RC generator, Agilent 54645A double channel storage oscilloscope, Agilent 82357A PC card, IEEE-488 communication cables and coaxial cables with BNC connectors (Kusák, Luňák).

To measure electric properties of two-pole and four-pole networks, a ZNC vector analyser made by Rohde & Schwarz can be used as a stand-alone analysing unit. The instrument is equipped, among others, with a SPEAG-made DAK-12 probe, which is primarily designed to measure and analyse the permittivity and its components.

The mentioned devices are integrated into an automated measuring unit.

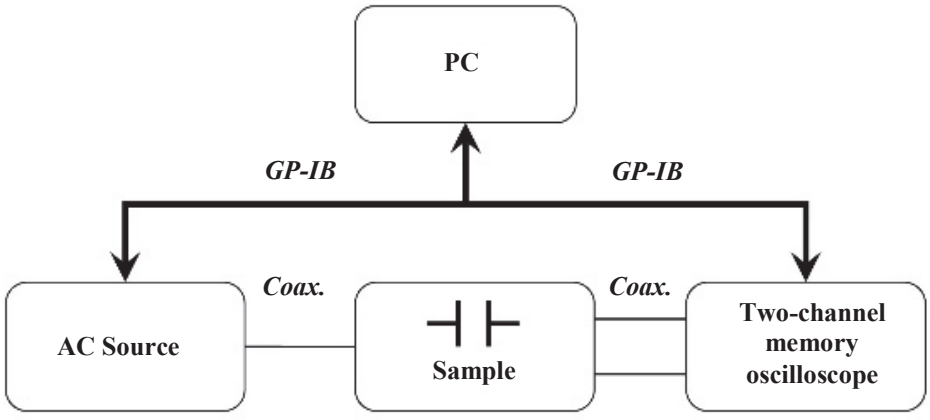

Fig. 7.1. Interconnection of Agilent 33220A RC generator, the specimen and the testing system by means of cables

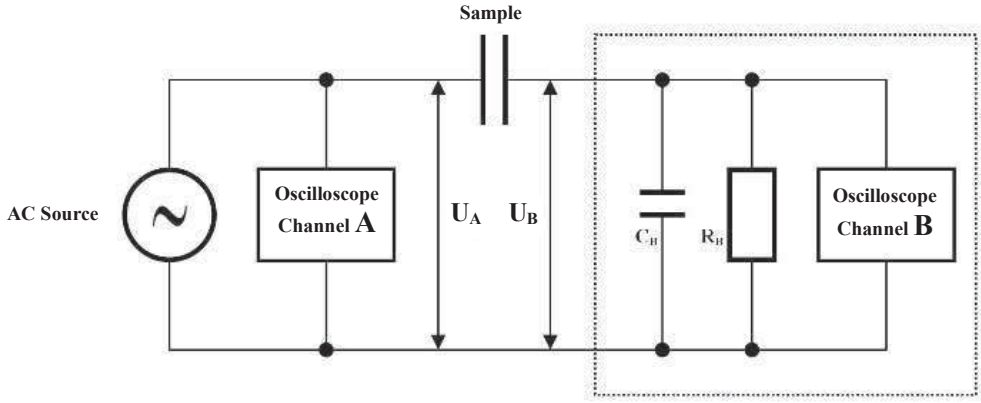

Fig. 7.2. Detailed instrument connection: AC voltage supply, specimen under test, double-channel oscilloscope (the dashed-line limited region indicates the oscilloscope B-channel input parameters)

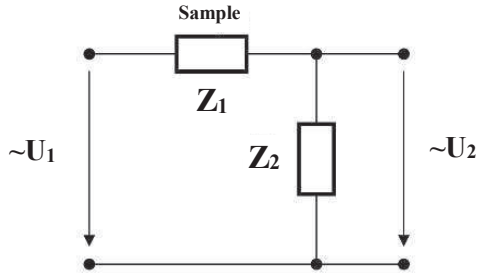

Fig. 7.3. A simplified circuit diagram.

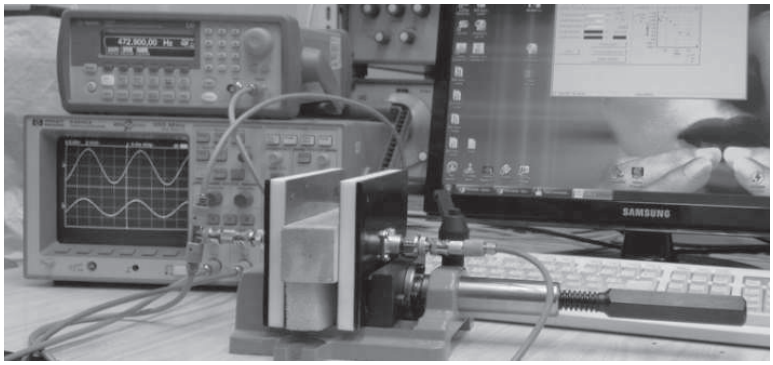

Fig. 7.4. The measuring setup: an AC voltage supply (Agilent 33220A RC generator), double channel oscilloscope, specimen under test in a fixture, and PC with a measuring software.

Depending on the branch of science employing IS, there are different variants of the measuring setup layout. In electrochemistry, the material is collected in electrochemical containers (cells), which are adapted for two-, three- and four-electrode measurements. In the thin film branch, conducting electrodes are deposited on the specimen under investigation, or, depending on the measured

specimen surface properties (conductivity, roughness), conducting pastes or coats of paint are used.

The fixture consists of an outer part, which is made of a steel section of appropriate seize and strength. From the outside, a borehole is drilled, around which a nut of chosen size is welded. A threaded rod with a handle passes through the nut. The threaded rod fits close on a metal bed, which is fastened to a metal slab by spot weld. The slab encircles a teflon plate to distribute the pressure from the screws over the teflon plate surface. The teflon plate is attached by means of small bolts. Opposite this teflon plate, another teflon plate is attached at the outer fastener. Brass plate electrodes are affixed to roughened inner surfaces of the teflon plates by means of a two-component adhesive. Lead-in cables are soldered with tin to the brass electrode outer sides to connect them to measuring instruments. Under both of the teflon plates, there is the third teflon plate.

The brass contact electrodes have an area of 3 x 10 cm. The thickness of the electrode brass sheet is 0.7 cm. The outer earthed shielding is made of the same brass sheets, which were connected to the frame by means of four M4 bolts and riveting nuts for each pressure plate. The brass electrodes were affixed to the roughened teflon surfaces by means of a two-component adhesive. The pressure steel plates have an area of 13.5 x 11 cm and a thickness of 4 mm. A teflon plate of the same area as the pressure plates and a thickness of 11.5 mm serves as an insulating element. The slab encircles a teflon plate to distribute the pressure from the screws over the teflon plate surface. The electrode lead-out wires are connected to an N-type flange-mounted coaxial connector. Taking into account a large number of coaxial cable terminations, the output can be modified to fit BNC, SMA, FME and other connectors. The frame of the whole fixture consists of a cast-iron vice with a threaded bar. The electrode pressure force on the specimen surface is being adjusted manually by the operator.

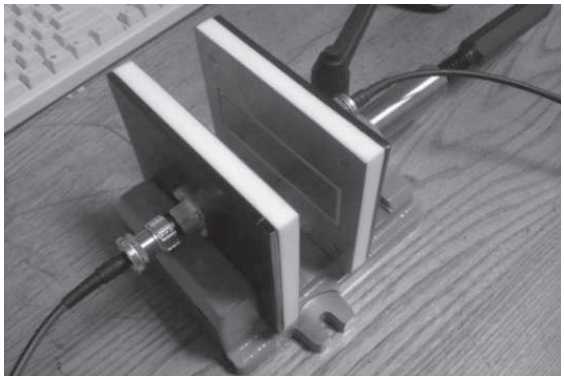

Fig. 7.5. Overall appearance of the fixture for applying plate electrodes to slab specimens of variable thickness

7.3. Formulas applied

To characterize polarization processes, the permittivity and the impedance are most frequently used in practical applications. As follows from the Maxwell's material equations (Szántó 2003), the permittivity is a proportionality constant between the electric field intensity vector and the electric induction vector. An analogous approach can be used when expressing the impedance and its components.

The formulas given below have already been rearranged to correspond to the circuit diagram with the particular measuring instruments used (Fig. 7.4).

In the impedance spectroscopy, the frequency dependence of the quantities in question is being evaluated on the basis of the voltage ratios and phase shifts between the oscilloscope A, B, inputs.

The measured gain L is defined as

$$L = 20 \log K \tag{7.1}$$

where $K=U_B/U_A$ (U_B, U_A are electric voltages in the B, A oscilloscope inputs, respectively). It appears that the system (specimen) of Fig. 7.3 is best represented by a parallel RC equivalent circuit.

The next step to take is therefore to express the phase of the impedance consisting of a precision resistor, R_B, and a precision capacitor, C_B, in B input of the phase and gain measuring instrument. It is

$$\varphi_B = -\arctan \omega R_B C_B \tag{7.2}$$

The impedance of the R_B, C_B parallel network in the B input of the phase measuring instrument is

$$Z_B = \frac{\sqrt{R_B^2 + (\omega R_B^2 C_B)^2}}{1 + (\omega R_B C_B)^2} \tag{7.3}$$

and the phase of the measured impedance Z is

$$\varphi_1 = \varphi_B + \arctan \frac{\sin \Delta\varphi}{\frac{U_B}{U_A} - \cos \Delta\varphi}. \tag{7.4}$$

The absolute value of the measured impedance will therefore be

$$Z = \frac{Z_B \cdot \sin \Delta\varphi}{\frac{U_B}{U_A} - \sin(\varphi_B - \varphi_1)}, \tag{7.5}$$

(Here, $\Delta\varphi$ is the phase shift between the A, B inputs of the double-channel oscilloscope, φ_1 –is the phase of the specimen under measurement).

The real and imaginary parts of the impedance Z are

$$\mathrm{Re}(Z) = Z \cdot \cos\varphi_1 \qquad \mathrm{Im}(Z) = Z \cdot \sin\varphi_1 . \tag{7.6}$$

Hence, the loss factor of the insulating material, which is defined as the ratio of the real and imaginary part of the impedance Z, is

$$\tan\delta = \frac{\mathrm{Re}(Z)}{\mathrm{Im}(Z)} = \frac{1}{\tan\varphi_1} . \tag{7.7}$$

Depending only on the material itself but not on the specimen geometry, the loss factor is a very important material constant.

The resistance of the parallel *RC* network representing the measured system then is

$$R = \mathrm{Re}(Z) \cdot (1 + \tan^2\varphi_1) . \tag{8.7}$$

and its capacity

$$C = -\frac{\tan\varphi_1}{\omega R} \tag{9.7}$$

A theory of dielectric polarization was formulated by Debye (MacDonald, J R 1987) for homogeneous materials. However, experiments carried out on real materials and the respective conclusions did not show to be in agreement with the fundamental theories. K S Cole and R H Cole and, also, Fuoss and Kirkwood, started from the Debye's theory to derive models of a dielectric which appear to fit experiment results and conclusions (Mentlík 2006) more closely. The behaviour of a dielectric in an AC electric field is best described in terms of the complex relative permittivity. Debye has derived a formula for the complex relative permittivity, ε^*, of weakly polar liquid dielectrics, as follows:

$$\varepsilon^*(j\omega) = \varepsilon_\infty + \frac{\varepsilon_s - \varepsilon_\infty}{1 + j\omega\tau}, \tag{7.10}$$

Here τ is the relaxation time, independent of the time, however dependent on the temperature, ε_s – static permittivity (frequency → 0 Hz), ε_∞ – optical permittivity (frequency → ∞ Hz), angular frequency $\omega=2\pi f$, f – frequency of the exciting electric field.

Following equation holds for the loss factor tan δ:

$$\tan\delta = \frac{\varepsilon''(\omega)}{\varepsilon'(\omega)} = -\frac{(\varepsilon_S - \varepsilon_\infty)\omega\tau}{\varepsilon_S + \varepsilon_\infty\omega^2\tau^2} . \tag{7.11}$$

There are several different relaxation times in a real dielectric. Their distribution is described by a distribution function. Exact determination of a suitable distribution function being difficult, an approximation by a properly selected analytical function is usually carried out. According to Cole's function, the complex relative permittivity can be expressed as follows:

$$\varepsilon^*(j\omega) = \varepsilon_\infty + \frac{\varepsilon_S - \varepsilon_\infty}{1 + (j\omega\tau_1)^{1-\alpha}}, \tag{7.12}$$

Here, τ_1 is the most probable relaxation time, around which the particular relaxation times are distributed according to a distribution function $f(\tau)$, where α is a distribution parameter ($0<\alpha<1$).

J R MacDonald suggested an equivalence between the complex relative permittivity as described by equations (10), (12), and the formulas for the complex impedance Z (MacDonald 1987). Formulas for the real and imaginary components of the complex relative permittivity have been derived and, based on the above mentioned equivalence, equations for the components of the complex specific impedance have been obtained (Barsoukov 2005).

Cole and Davidson have expressed the complex relative permittivity by squaring the whole numerator in formula (12) ($0<\gamma<1$).

$$\varepsilon^*(j\omega) = \varepsilon_\infty + \frac{\varepsilon_S - \varepsilon_\infty}{(1 + j\omega\tau_1)^{\gamma}} \tag{7.13}$$

Havriliak and Negami have put forward a new formula for ε^*, which is, according to their literature search, applicable to complex structure materials (MacDonald 1987).

$$\varepsilon^*(j\omega) = \varepsilon_\infty + \frac{\varepsilon_S - \varepsilon_\infty}{(1 + (j\omega\tau_1)^{1-\alpha})^{\beta}} \tag{7.14}$$

Here, α is a parameter, characterizing the width of the relaxation spectrum ($0<\alpha<1$), β is a parameter characterizing the dispersion curve asymmetry ($0<\beta<1$). The behaviour of a dielectric can now be described by means of five parameters, namely, ε_s, ε_∞, α, β, τ_1; unfortunately, their determination is rather difficult (MacDonald 1987).

Using an appropriate software package, parameters of the three model types will be searched for the material under investigation. The degree of correlation between the model and experiment properties is expressed by means of Pearson's correlation coefficient r.

7.4. Modelling on the basis of ceramic shard specimen measurement results

The ceramic shard specimens have been manufactured using Chvaletice fly ash, their firing temperature being 1 050 °C. The firing losses amounted to 11.2 %. The volume density was about 2 005 kg/m^3. The water absorption capacity: 7.5 %. The bending strength: 24.7 MPa. The grain size distribution: about 5 % on a 0.063 mm sieve. The different specimens differed in the admixture only. The specimen thickness was 10 mm.

Brass plates of a surface area of 40x23 mm, which are pressed against the specimen surface by means of a screw fixture, were used to interface the specimen.

Admixtures

Bentonite ($Al_2O_3.4SiO_2.nH_2O$) - clay. It is a white to light-yellow powder material featuring a specific chemical composition. It is used as ceramics plasticizing agent in the ceramic industry. In this research, a non-activated bentonite, in which the calcium and magnesium ions have not been replaced by activation by sodium ions, has been used. The apparent volume density was 936 kg/m3, pH = 8.7.

Sodium water glass Na_2SiO_3 of a silicate module of 1.6 and a density of 1 560 kg.m^{-3} has been used to prepare the specimens.

Phosphoric acid - application of H_3PO_4 to aluminates results in the generation of aluminium phosphates - $AlPO_4$, which are decomposing at temperatures over 1 500 °C, giving rise to P_2O_5, which escapes. Mechanical properties improve with growing temperature, particularly, in the presence of Cr_2O_3 (Tupy, M).

The loss factor is a material characteristic, whereas the remaining two quantities are related to the specimen type in question only. Prior to the model application, the values of the variables (ReZ, ImZ) have been divided by the specimen thickness and multiplied by the electrode surface area (it is assumed that only the electric field in the space between the electrodes plays the role; in view of the high material resistivity, the effect of the field beyond the electrodes is neglected). In this way, specific resistance (Real $z(f)$, Re $z(f)$) and reactance (Imag $z(f)$, Im z(f)) versus frequency plots have been obtained for the material under investigation. At the same time, from our readings of (Re$Z(f)$, Im$Z(f)$, the real ($\varepsilon_{real}(f)$) and imaginary ($\varepsilon_{imag}(f)$ components of the complex relative permittivity versus frequency functions have been derived and calculated, which have also been modelled (having been denoted ε' a ε'' formerly). In what follows, the complex relative permittivity will also be briefly termed the complex permittivity.

Three types of the model will be distinguished. Model No. 1 – based on mathematical formula 12, model No. 2 – based on method No. 13, model No. 3 – based on mathematical formula 14. The parameter τ_1, which appears in the mentioned terms, will be designated τ.

The measurements were carried out at common laboratory conditions (room temperature, 24 °C, air humidity, 30 %, atmospheric pressure, 1 000 hPa approximately), silver-based conducting paint was not spread over the specimen faces.

The different specimens are referred to in an abbreviated way, the admixture, which is characteristic for each specimen, being mentioned in the specimen designation (bentonite 5 %, bentonite 10 %, phosphoric acid, water glass, etc.).

Over 50 points have been obtained for each characterization. The measurements were carried out at frequencies ranging from 40 Hz to 1 MHz .

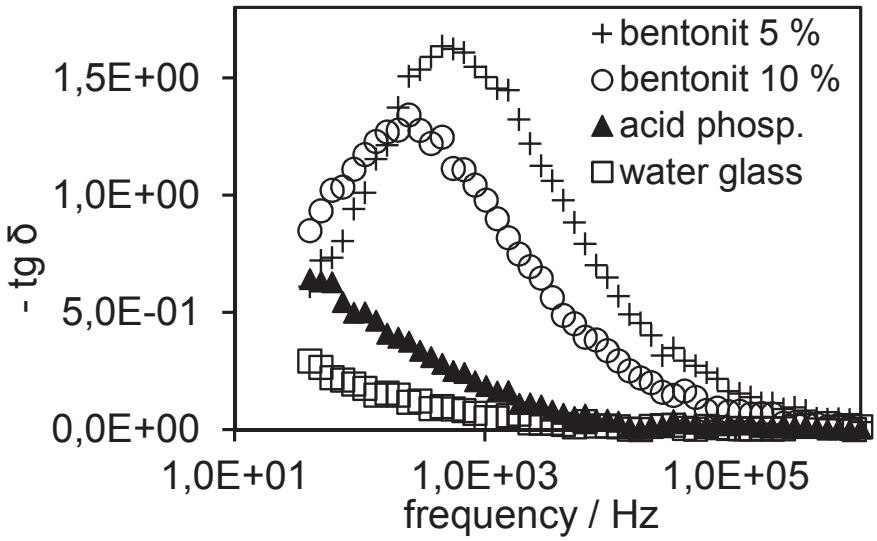

Fig. 7.6. Loss factor versus frequency plots for all ceramic specimens

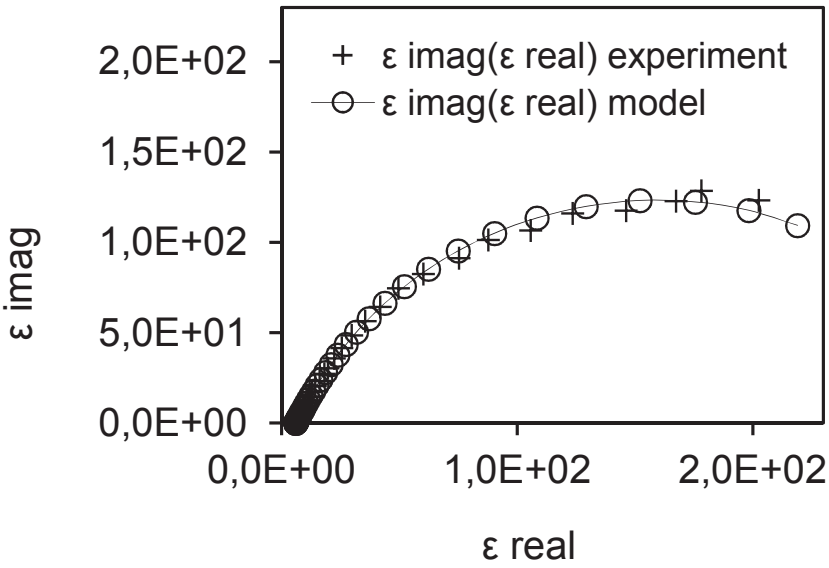

Fig. 7.7. Measured and model plots of the complex permittivity imaginary component versus the complex permittivity real component. 5 % of bentonite containing ceramics. Model type 2, based on the loss factor spectrum shape best fit.

Heavy differences are apparent in the spectra of ceramics specimens featuring different admixtures (see Fig 7.6). The loss factor is minimum for water-glass-admixtured ceramics. From this function frequency-upwards, the difference from the same function for a phosphoric-acid-admixtured specimen is steadily decreasing with growing frequency. Local peaks are observed in ceramics with bentonite, higher peaks being observed for 5 % of bentonite. The peaks occur at different frequencies of the electric voltage. The last two mentioned spectra show slight imperfections in the curve continuity. As they are observed at different frequencies, the spectrum imperfections are not attributed to a measuring instrument effect. Resonance or damping effects, which depend on the excitation signal frequency, may have caused the mentioned irregularities of the spectra. However, the presence of another local peak cannot be foreclosed, another relaxation time may also be assumed.

Table. 7.1. Model parameter values for the loss factor spectrum of ceramics specimen with admixture. Model type: 1. Here, ε_∞ denotes the optical permittivity, ε_s, the static permittivity.

No.	approx. spectrum	parameter	Material				unit	Note:
			Admixtured ceramics					
			bent. 5 %	bent. 10 %	phosph. acid	water glass		
1	tg $\delta(f)$	ε_∞	6.1	6.7	4.9	6.5	-	**model 1**
2		ε_s	361	272	73	58	-	
3		τ	0.003	0.007	0.092	0.5	s	
4		α	0.206	0.25	0.369	0.433	-	
5		r	0.9979	0.999	0.9977	0.992	-	

The optical permittivity values obtained from ceramics specimens containing 5 % of bentonite and 10 % of bentonite do not correspond to the relative permittivity values obtained from our preliminary measurements. For a 5 % admixture of bentonite, the relative permittivity was 20 at 100 Hz, for 10 % of bentonite, the same quantity featured a value of 15 at 100 Hz. If phosphoric acid was added, the relative permittivity equalled 5, for a water-glass-admixtured ceramics, the value dropped to 4. In these cases, the optical permittivity values are closer to the preliminary values than in the case of bentonite-admixtured ceramics. This may be connected with the presence of a peak in the loss factor spectrum of bentonite-admixtured ceramics.

Now, we are going to apply the type 2 model to the same experimental data set.

The model spectrum of Fig. 7.7 is decreasing more abruptly at the lowest frequencies than in the case of model 1 spectrum. The match is not ideal in this region. However, it has been retained, for the sake of a better fit in the higher frequency region. A slight rectification of the curve is apparent at higher frequencies, however, it is not perceptible in the coordinate system used. Our selection of the specimen characterization method starting as low as 40 Hz proved to be suitable and advantageous. In this way, errors in the spectrum shape can be easily eliminated, particularly in the region of maximum values of the imaginary component of the complex relative permittivity.

Based on a different model, we have obtained almost identical values of the optical permittivity, namely, from the loss factor spectrum. The γ parameter is almost identical for bentonite-admixtured ceramic specimens. The correlation coefficient values are distinctly lower than in the cases mentioned before for most of our best-fit approximations.

Table 7.2. Model parameter values for ceramics specimen loss factor spectrum. Model type. 2. Here, ε∞ denotes the optical permittivity, εs, the static permittivity.

No.	approx. spectrum	Parameter	Material				unit	Note:
			Admixtured ceramics					
			bent. 5 %	bent. 10 %	phosphor acid	water glass		
1	tg $\delta(f)$	ε_∞	6	6.5	5	6.4	-	**model 2**
2		ε_s	286	152	250	27	-	
3		τ	0.003	0.004	1.11	0.1	s	
4		γ	0.757	0.765	0.586	0.589	-	
5		r	0.9983	0.9941	0.9971	0.9921	-	

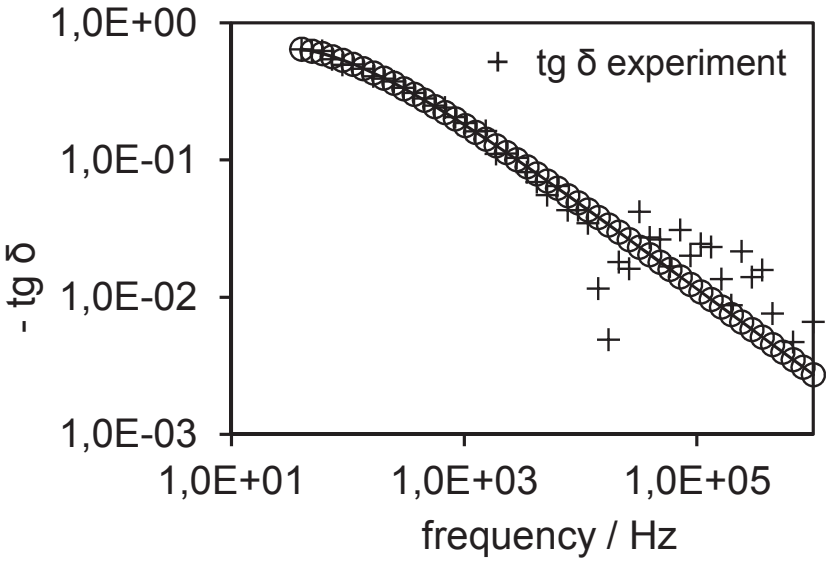

Fig. 7.8. Loss factor versus frequency plot for a phosphoric-acid-admixtured ceramics. Model type: 3. Together with a model curve. Both axis values are plotted in logarithmic coordinates.

Finally, let us present the 3rd model based modelling. As an example, we take the loss factor spectrum for a specimen of ceramics with a phosphoric acid admixture.

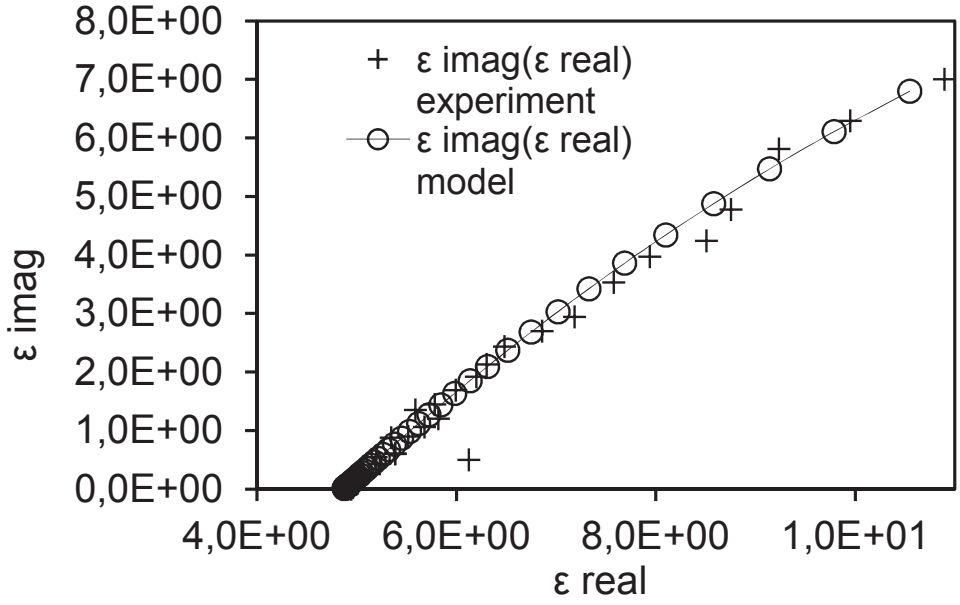

Fig. 7.9. Measured and model plots of the complex permittivity imaginary component versus the complex permittivity real component. Phosphoric-acid-admixtured ceramics. Model type: 3, based on the loss factor spectrum shape best fit.

Fig. 7.8 illustrates the measured value spread on the loss factor curve for a phosphoric acid admixtured ceramics at the lowest loss factor values. Logarithmic scale coordinate axes. The spread takes place at higher frequencies.

The complex relative permittivity imaginary component versus real component diagram is substantially rectified in comparison with the same diagram of bentonite-admixtured ceramic (not shown here). Measured values are slightly scattered around the model curve throughout the spectrum. The complex permittivity component values do not exceed 10. The first estimate of the optical permittivity can be found based on the position of the curve virtual intersection with the real component axis.

Table 7.3. Model parameter values for ceramics specimen loss factor spectrum and complex permittivity value spectrum for ceramics specimens. Model type: 3. Here, ε_∞ denotes the optical permittivity, ε_s, the static permittivity.

No.	Approx. spectrum	Parameter	material				unit	Note:
			Admixtured ceramics					
			bent. 5 %	bent. 10 %	phosph acid	water glass		
1	tg $\delta(f)$	ε_∞	6.1	6.7	4.9	6.3	-	**model 3**
2		ε_s	320	215	36	19	-	
3		τ	0.003	0.007	0.029	0.036	s	
4		α	0.148	0.126	0.096	0.16	-	
5		β	0.928	0.809	0.693	0.65	-	
6		r	0.9986	0.9989	0.9976	0.988	-	
7	Real $\varepsilon(f)$	ε_∞	6.2	6	4.9	6.5	-	
8		ε_s	313	208	49	45	-	
9		τ	0.003	0.006	0.04	0.069	s	
10		α	0.161	0.12	0.252	0.124	-	
11		β	0.969	0.86	0.857	0.829	-	
12		r	0.9996	0.9991	0.9941	0.9813	-	

The optical permittivity values feature the same magnitudes as those of the previously mentioned models, whereas the static permittivity values are different. The most probable relaxation times, as resulting from our measurements, are substantially different, first of all, for no-bentonite ceramics specimens.

The α parameter nears 0.1 for all ceramics specimens, giving evidence of a rather higher width of the relaxation time distribution curve. The lower value pertaining to phosphoric-acid-admixtures ceramics specimens is in a good agreement with our expectations, taking into account the loss factor versus frequency plot shape. The same parameter value, as measured on water-glass-admixtured specimens, is slightly higher than for the other specimens, which would mean a construction of the relaxation time spectrum. Such a conjecture cannot be ruled out, in view of the probable position of the loss factor peak deep in the low-frequency region.

The β parameter tends to unity for a 5 %-bentonite ceramics. For the remaining specimens, this parameter has lower but still relatively high values. This would support the hypothesis of a high symmetry of the relaxation time distribution. The values of this parameter, as determined from the loss factor spectrum, are in

a good agreement with the values, which have been determined from the complex relative permittivity real component curves.

Application of model No. 3 to the complex relative permittivity imaginary component versus frequency has not resulted in any satisfactory agreement with the experiment. No realistic physical results have been obtained in the case of 10 %-bentonite ceramics.

7.5. Conclusions

Non-destructive testing (NDT) of construction materials by means of electric methods is a rarely used technique. For alternating electric fields, a method consisting in impedance measurements at different exciting frequencies was successfully used. The impedance spectroscopy is not applicable to materials featuring a high electric resistance, due to the part dimensions and slit formation impracticability.

Being characterized by the impedance spectroscopy method, the specimens featured differences in the loss factor spectra which appeared to depend on the frequency. Thanks to the application of three model types of the dielectric, we managed to get the values of ε_s, ε_∞, α, β, γ, τ parameters. The regression coefficient reached a maximum value for model No. 1, being followed by model No. 3. The lowest value was shown by model No. 2.

The model of the dielectric proved to be best suited for bentonite-admixtured ceramic bodies' characteristics.

Acknowledgment

This paper has been worked out under the project GAČR No. 16-02261S and project LO1408 "AdMaS UP - Advanced Materials, Structures and Technologies", supported by Ministry of Education, Youth and Sports under the „National Sustainability Programme I".

References

Barsoukov E., MacDonald J. R., *Impedance spectroscopy: theory, experiment, and applications*. 2nd ed. /. Hoboken, N.J.: Wiley-Interscience, 2005, xvii, 595 p.

Kocman V. *Fyzika a technologie elektrotechnických materiálů - Izolanty A.* Praha: SNTL - Nakladatelství technické literatury, 1971, 526 p.

Kusak I., Lunak M., Schauer P. *Tracing of Concrete Hydration by Means of Impedance Spectroscopy (New Tool for Building Elements Testing*), Applied Mechanics and Materials, 2013, vol. 248, pp. 370-378.

MacDonald J. R., *Impedance spectroscopy, emphasizing solid materials and systems*, Bibliography, Canada 1987, 346 p.

Mentlik V., *Dielektrické prvky a systémy, BEN* – technická literatura, Praha 2006, 240 p.

Palai-Dany T., Dielektrická spektroskopie karboxymetylcelulózy v časové oblasti. *Brno: Vysoké učení technické v Brně, Fakulta elektrotechniky a komunikačních technologií*, 140 s. Vedoucí disertační práce Doc. Ing. Karel Liedermann, CSc, 2009,.

Szántó L, *Maxwellovy rovnice a jejich názorné odvození*. BEN – technická literatura, Plzeň, 112 p, 2003.

Tupy M., Sotiriadis K., Kusak I., Lunak M., Stefkova D., Petranek V., *Exposure of Mortars Modified with Rubber Aggregates and Polymer Admixtures to Acid Environments and Elevated Temperature Conditions,* Journal of Materials in Civil Engineering, American Society of Civil Engineers (ASCE), United States, 2015, vol. 28, pp. 91-99.